Satellite-Retrieved Microstructure of AgI Seeding Tracks in Supercooled Layer Clouds

DANIEL ROSENFELD

Institute of Earth Sciences, The Hebrew University of Jerusalem, Jerusalem, Israel

XING YU AND JIN DAI

Meteorological Institute of Shaanxi Province, Xi'an, China

(Manuscript received 23 June 2004, in final form 18 October 2004)

ABSTRACT

NOAA Advanced Very High Resolution Radiometer (AVHRR) images revealed conspicuous tracks of glaciated cloud in thick supercooled layer clouds over central China. These tracks were identified as being artificially produced by cloud-seeding operations at the −10°C isotherm, less than 1 km below cloud tops, aimed at precipitation enhancement, by means of AgI acetone generators. The cloud composition was deduced by retrieving the cloud-top effective radius (r_e) and analyzing its spatial relations with cloud-top temperatures and with the visible reflectance. Cloud-top temperature varied between −13° and −17°C. The glaciation became apparent at cloud tops about 22 min after seeding. The glaciated tops sank and formed a channel in the supercooled layer cloud. The rate of sinking of about 40 cm s^{-1} is compatible with the fall velocity of ice crystals that are likely to form at these conditions. A thin line of new water clouds formed in the middle of the channel of the seeded track between 38 and 63 min after seeding, probably as a result of rising motions induced by the released latent heat of freezing. These clouds disappeared in the more mature segments of the seeded track, which continued to expand throughout the observation period of more than 80 min. Eventually the seeding tracks started to dissipate by expansion of the ambient cloud tops inward from the sides. Using the brightness temperature difference between 10.8 and 12.0 μm allowed for observation of the seeding signature deep in the clouds, even when it was obscured under thin supercooled layer clouds. This is the third and most detailed report of effects of advertent cloud seeding for precipitation enhancement being detected and analyzed based on satellite observations. It opens new possibilities of using satellites for directing and monitoring weather modification experiments and operations.

1. Introduction

Modern research into cloud seeding began in 1946, when Vincent Schaefer of General Electric noticed that a small piece of solid carbon dioxide (dry ice) could generate a large number of ice crystals in a laboratory-generated supercooled fog (Schaefer 1946). He then went up in a small aircraft and dropped crushed dry ice into supercooled stratocumulus clouds over western Massachusetts, and found that snow crystals did, indeed, fall out from the cloud, leaving a hole where the cloud water was altered into ice precipitation, such as shown in Fig. 1. In the following year, Bernard Vonnegut of General Electric found that particles of silver iodide could also generate large numbers of ice crystals if the cloud is colder than about −5°C. Many similar experiments have been carried out subsequently, showing that seeding supercooled layer clouds with depths smaller than 1 km could leave a cleared track that could reach a width of 3 km in 35 min and exist for more than 2 h. Seeding of thicker layer clouds had caused glaciation but often was not able to cause holes in the clouds (Langmuir 1961a,b; Mason 1962). These observations provided solid evidence of the microphysical effects of cloud seeding in thin supercooled layer clouds. The thin layer clouds had too little water for producing any significant surface precipitation. However, the observed effects on these clouds were used as justification for seeding operations that began on much thicker clouds with the hope that it would result in precipitation enhancement. Precipitation-forming processes in the deeper and more convective clouds are much more complex and posed a much greater challenge in documenting the seeding microphysical signatures in conjunction with the statistical documentation of added precipitation on the ground.

Corresponding author address: Prof. Daniel Rosenfeld, Institute of Earth Sciences, The Hebrew University of Jerusalem, Jerusalem 91904, Israel.
E-mail: daniel.rosenfeld@huji.ac.il

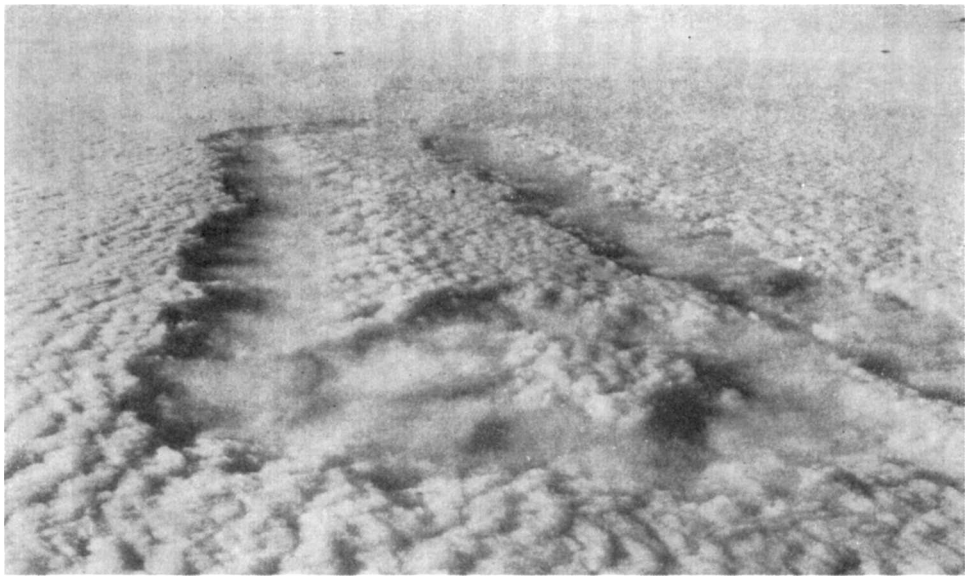

FIG. 1. The general view of the dry-ice-seeded racetrack pattern in supercooled cloud layer 37 min after the start of the seeding and 24 min after the end of the seeding. The cloud layer extended between 4500 and 6800 ft over Utica, NY, with a top temperature of −5.6°C. The picture was taken at 1521 UTC 24 Nov 1948 from an altitude of 17 630 ft. (From Langmuir 1961b.)

Each of the two was achieved separately, but their combination that is necessary for scientific proof of the efficacy of cloud seeding for precipitation enhancement has not yet been achieved (Silverman 2001).

The visually observed seeding tracks provided the basis for embarking on extensive cloud-seeding projects for rain enhancement. Forty years later a similar development occurred, when the discovery of satellite-observed ship tracks in thin marine layer clouds brought to our awareness the coalescence-suppressing effects of the pollution aerosols from the stacks of ships (Albrecht 1989). This triggered the current era of intense research of the role of cloud–aerosol interactions on drizzle, cloud optical properties and impacts on the Earth radiation budget, and climate implications. The analog to rain enhancement by cloud seeding was the rain suppression by air pollution from clouds that are much deeper than the marine stratus layer. Insights to this became possible when satellite methodology was developed to infer the relation between the vertical evolution of the cloud microstructure and precipitation-forming processes in convective clouds (Rosenfeld and Lensky 1998). This methodology was applied to obtain evidence of precipitation suppression by smoke from forest fires (Rosenfeld 1999) and by urban and industrial air pollution (Rosenfeld 2000), and the way by which large salt aerosols can restore the precipitation (Rosenfeld et al. 2002; Rudich et al. 2002).

The pollution impacts on cloud microstructure and precipitation can be considered as inadvertent cloud seeding that can be clearly visible from satellites. We are aware of two previous probable advertent glaciogenic seeding signatures in convective clouds (Woodley et al. 2000, and Fig. 13 in Rosenfeld and Woodley 2003). Yu et al. (2005) present a seeding track at the top of deep supercooled layer clouds that can be traced exactly to the aircraft trajectory and document the correspondence between the dispersion of the seeding material and the horizontal extent of the seeding track. In this study we analyze quantitatively the satellite data to obtain further physical insights to the seeding effects in this case, in what appears to be one of the first steps toward satellite applications to advertent weather modification.

2. Satellite observations

The *National Oceanic and Atmospheric Administration* (*NOAA*)*-14* Advanced Very High Resolution Radiometer (AVHRR) High Resolution Picture Transmission (HRPT) data from 0735 UTC 14 March 2000 were processed and rendered (Fig. 2a and Fig. 3) according to the microphysical scheme of Rosenfeld and Lensky (1998). The seeding track appears conspicuously in red, imbedded in the ambient supercooled layer clouds in yellow and orange colors. The times and coordinates of the flight track of the seeder aircraft are given in Table 1 and marked on Fig. 3. The aircraft ascended to the altitude of 4000 m while circling near point O. Then it started seeding at point A, flying generally westward (from right to left in Figs. 2 and 3) on a zigzag line; its turning points are marked by the char-

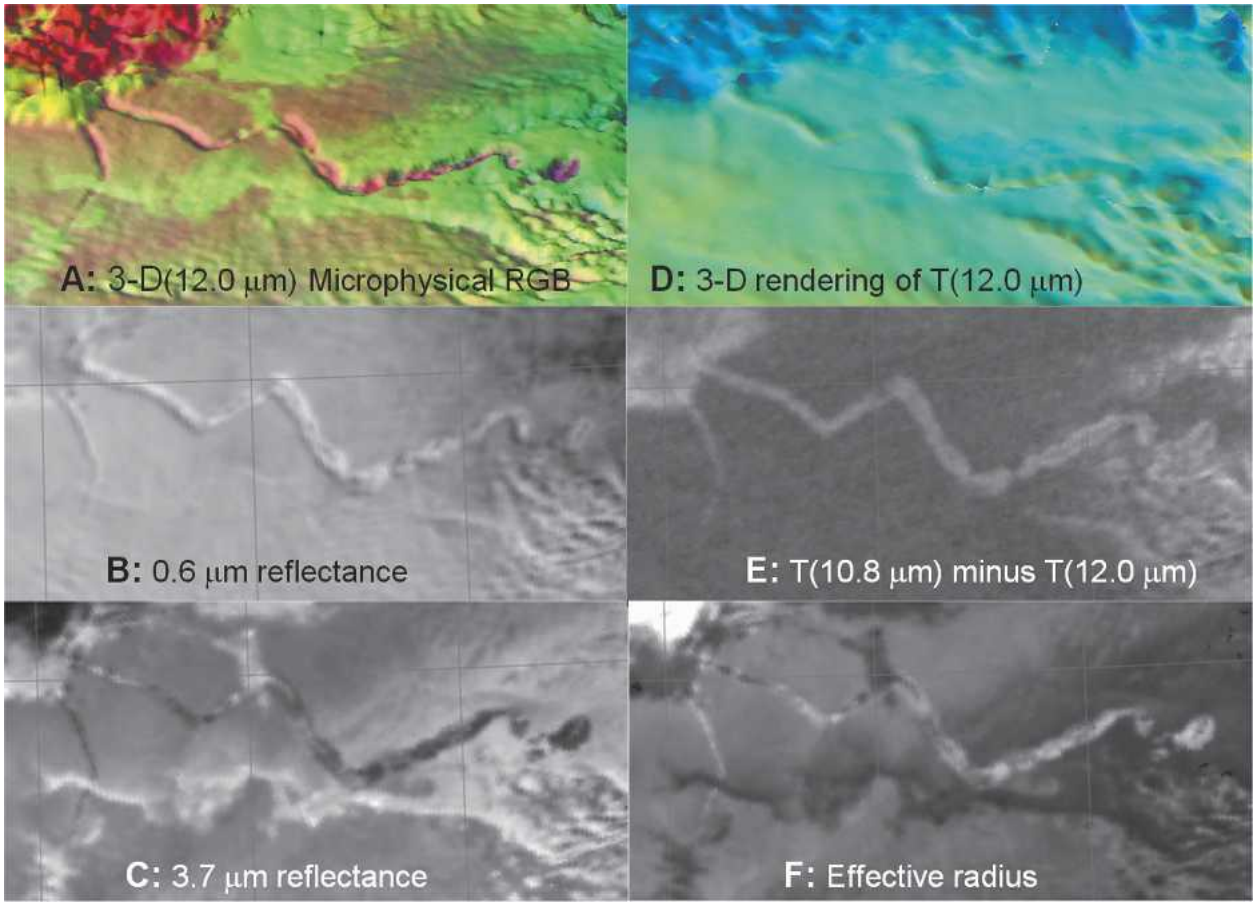

FIG. 2. *NOAA-14* AVHRR microphysical rendering of the seeding track over central China on 0735 UTC 14 Mar 2000. The aircraft flew generally westward, that is, from right to left, so that the seeding track becomes older from left to right. (a) The color composite is red for the visible reflectance, green for the 3.7-μm reflectance component, and blue for the 10.8-μm brightness temperature, according to the scheme of Rosenfeld and Lensky (1998). The surface is rendered in a topographic-like image, where the height is determined by the 12.0-μm cloud-top brightness temperature. Lower temperatures are shown as a higher surface, in accordance with the decreasing cloud-top temperature with an increasing cloud-top height. The top of a supercooled layer cloud is indicated by the yellow color, whereas the glaciated seeding track is marked by the red track in the clouds. The following other cloud properties are shown: (b) 0.6-μm reflectance; (c) 3.7-μm reflectance, where darker indicates larger cloud drops or ice cloud; (d) relief rendering of the 12.0-μm cloud-top brightness temperature, with colder being bluer; (e) 10.8-μm minus 12.0-μm brightness temperature difference, where larger values are brighter and indicate thinner clouds; (f) cloud particle effective radius, where brighter indicates larger values.

acters B–H. The aircraft seeded point A 80 min before the satellite overpass time. The seeded track became younger from points A to H. The seeder aircraft passed through point H 15 min after that satellite overpass. The cloud-seeding flight time from A to H lasted 66 min, consuming 880 g of AgI. The seeding rate was 0.222 g s^{-1}. The formula of the operational seeding material is as follows (the unit is grams): AgI, 20; NH_4I, 6.2; Acetone 879 (1111 mL); water, 50; NH_4ClO_4, 3.0; and $NaClO_4$, 41.7, forming a concentration of ~2% acetone solution of AgI.

To fully understand the composite image, it is necessary first to interpret the information of the individual AVHRR channels and some additional fields produced by them. According to the visible image (Fig. 2b) the seeding appears to have produced a channel in the cloud tops; it is obvious by the shadow structures in the visible image. Using the length of the shadows to calculate the depth of the channel results in a depth of 700 m at cross section 9 (see markings on Fig. 3), deepening to about 1300 m at cross section 7, remaining about this depth to cross section 5 and deepening to about 1500 m at cross section 2. As expected for the lower tops, they were also warmer. The channel is, therefore, visible also in the cloud-top temperature map of 12.0-μm brightness temperature, illustrated in Fig. 2d. The 12.0-μm brightness temperature is selected because the clouds have greater emissivity at this wavelength as compared with 10.8 μm. With little water vapor above the cloud tops, as is the case here, the 12.0-μm bright-

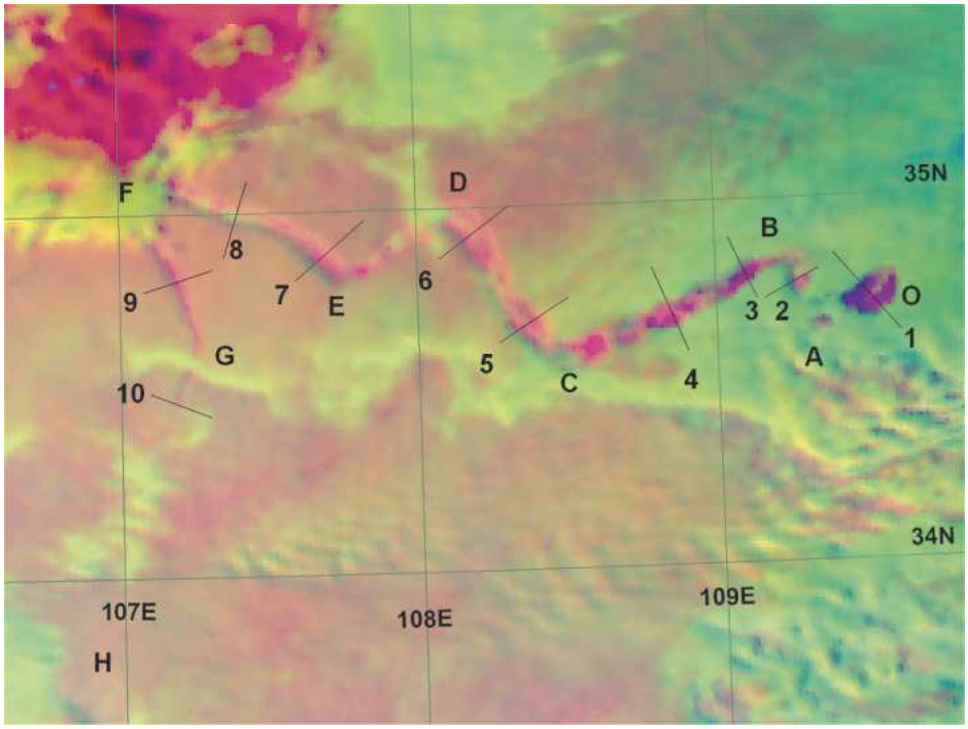

FIG. 3. Same as Fig. 2a, but for a larger area, without the 3D rendering. The characters are the locations along the seeding trajectory as shown in the companion paper of Yu et al. (2005). The numbered lines mark the locations of the cross sections shown in Fig. 3.

ness temperature is closer to the actual cloud-top temperature than at 10.8 μm. According to this, cloud-top temperature in the channel became progressively warmer with respect to the ambient cloud by 0.4°, 0.9°, and 1.2°C for cross sections 9, 7, and 5, respectively (see Fig. 4). The value reached 1.5°C in segment AB. This trend of cloud-top warming in the seeded track continued with its increasing age to a difference of 2.5° and 4.0°C in cross sections 4 and 1, respectively.

The ambient clouds had particle effective radius of 10–15 μm and top temperatures from −13° to −17°C. The methodology of Rosenfeld and Lensky (1998) implies that cloud tops were supercooled on the verge of drizzling and/or being of a mixed phase composition. The seeder aircraft was not equipped with a cloud physics probe, but after landing the aircraft was still coated in places with a thick layer of ice, indicating that it flew through severe icing conditions during much of its seeding mission. The composition of the cloud within the seeding track was ice, as indicated by the strong absorption of the solar reflectance component of 3.7 μm (Fig. 2c) that resulted in a large indicated effective radius of the cloud-top particle (Fig. 2f) that appears bright. The typical size of ice particles that form in mixed phase clouds is much larger than 10–15 μm, and they appear even larger when the cloud particle effective radius is retrieved with the algorithm for water droplets, as done in this study. Therefore, this combination of a relatively small effective radius and low temperatures indicate that the ambient clouds are composed of supercooled droplets, possibly with low concentrations of ice particles. This suggests that the seeded cloud volume glaciated into ice hydrometeors that precipitated, and so lowered the cloud-top height. According to the shadow length and the temperature difference, the depth of the channel in the clouds increased with the age along the

TABLE 1. The report of the seeder aircraft. Time of reported seeding initiation is 0615 UTC. The time of the satellite overpass is 0735 UTC.

Time (UTC)	Minutes before satellite	Place	Altitude (m)	Speed (km h^{-1})
0558	97	O (34°24′, 109°14′)	2200	
0615	80	A (34°18′, 108°56′)	4000	400
0619	76	B (34°24′, 108°43′)	4000	400
0633	62	C (34°15′, 108°13′)	4350	400
0642	53	D (34°41′, 107°47′)	4350	300
0648	47	E (34°31′, 107°23′)	4350	300
0659	36	F (34°54′, 106°50′)	4350	320
0708	27	G (34°21′, 107°08′)	4350	320
0721	14	H (33°38′, 106°56′)	4350	320
0735	0	I (33°19′, 106°09′)	4350	320

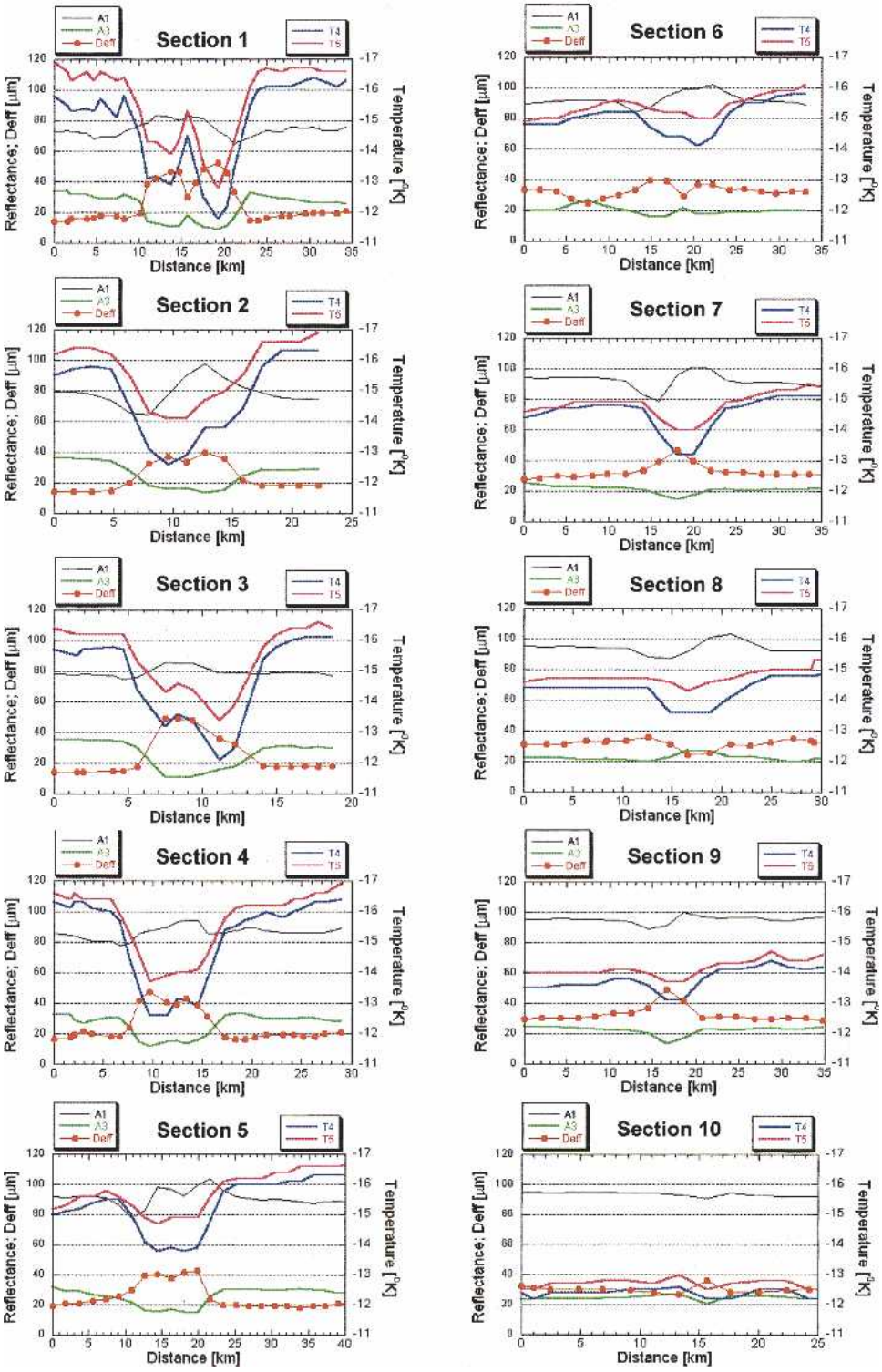

FIG. 4. Cross sections across the seeding tracks, at the respective numbered lines in Fig. 3. The left ordinate scales the reflectance at 0.6-μm (A1, black) and 3.7-μm (A3, green) channels, and the cloud-top particle effective diameter (Deff, red line with full circles at each satellite pixel). The right ordinate scales the brightness temperatures at 10.8-μm (T4, blue line) and 12.0-μm (T5, purple line) channels. Note the gradual widening of the seeding track as it matures from section 10 to 1, as indicated by the decreased 3.7-μm reflectance, increased r_e, increased cloud-top temperatures, and the increased brightness temperature difference.

whole track, reaching about 1.5 km near point A. The aircraft-reported cloud thickness from the visible base to the top was 2.3–2.8 km, so that there was still 0.8–1.3-km-thick cloud depth left below the channel.

The decreased cloud thickness is revealed also by the brightness temperature difference (BTD) of 10.8- and 12.0-μm channels shown in Fig. 2e. The BTD is near zero for opaque clouds with cold tops. However, when the clouds become sufficiently thin or lose their water, upwelling radiation from the warmer objects below the clouds penetrates them and increases the brightness temperature that is measured by the satellite instruments. Because 10.8 μm is more transparent to the thermal radiation than the 12.0-μm channel, it will appear as having larger brightness temperature, so that the BTD would increase for less opaque clouds and for greater thermal contrast with the underlying surface (Inoue 1989). The BTD of the ambient clouds was 0.2–0.3 K, indicating that they were quite opaque and thick. The BTD within the seeded track decreased with some lag after the glaciation, showing no decrease in the newly glaciated track in cross section 10. At cross section 9 the BTD already increased to 0.7 K and kept increasing gradually to 1.3 K at point A. Apparently, the seeding track in the BTD image (Fig. 2e) is slightly obscured by thin layer clouds that occur above it. The seeded track can be seen under the higher thin supercooled cloud layer near point F. Indeed, the seeder aircraft crew reported having seen thin layer clouds above them in that vicinity.

The color composite image (Fig. 2a and Fig. 3) highlights the cloud-top microstructure and shows the sharp contrast between the flat-top supercooled layer clouds and the glaciated clouds in the seeded track. It appears that thin, new bright yellow clouds, which are supercooled water clouds with very small drops, formed inside the channel of the seeded track between points F and C.

The evidence that the seeded cloud became thinner comes from the visible image showing a channel (Fig. 2b), the warming of the cloud tops in the seeded track (Fig. 2d), and the increase of BTD in the seeded track (Fig. 2e). The seeded cloud became thinner apparently because the cloud top descended and it lost water to precipitation throughout its depth. The seeding track shows in BTD through the thin water clouds that obscure some of the segments. The seeding track becomes wider all the way to point A in the BTD image. This suggests that the narrowing of the seeding track in the visible image (Figs. 2a, 2b, and 3) is due to spreading of the preexisting water clouds from the sides closing above the channel of the seeding tracks. This is evident visually in Fig. 2a.

The clouds that close on the seeding track from its sides in its older parts are not reformed, but, rather, are the spreading of the old preexisting cloud matter. This is supported by the larger cloud particle size than that of the new clouds that formed in the middle of the seeded track, as shown in cross section 6 of Fig. 4. This is seen also qualitatively in the brighter 3.7-μm reflectance of these clouds on the dark background of the seeding track (Fig. 2c), as compared with the darker color of the ambient water clouds outside the channel.

3. Synoptic situation

The 500-hPa (Fig. 5a) map shows a tilted short wave with its axis just to the west of the study area. A cold front with air from a cold anticyclone swept through the seeded area moving from northwest to southeast ahead of the upper-trough axis, replacing light variable surface winds with moderate northerly winds, and dropping the temperatures by about 10°C, changing the widespread regional light precipitation from rain to snow (Fig. 5b). The region was overcast with low and medium clouds that were much wider than could be ascribed to the surface cold front. The relation of the isotherms and the 500-hPa surface suggest that these clouds were caused by warm advection of air that is lifted with the general rising motion at the eastern flank of the upper trough.

4. Physical interpretation

Multispectral analysis of NOAA AVHRR data was able to detect clearly the structural and microphysical changes in a seeded track within supercooled layer clouds, as induced by an operational cloud-seeding aircraft mission with the AgI acetone burner. Comparison of the seeded track with the aircraft reports (Table 1) of the marked locations on Fig. 3 allow us to time the age of the various segments of the seeded track (Yu et al. 2005). The seeded track appears about 22 min after seeding (to the south of point G along line GH in Fig. 3). Its first manifestation is the reduced reflectance at 3.7 μm, which reflects the onset of glaciation to the point of being discernable by the satellite. Soon after that the visible cloud tops appear to start sinking, as seen just to the south of the location of point G in Fig. 2b. This starts to appear as warming of the cloud-top temperature at about 27 min after seeding, or 5 min after the satellite-detected onset of glaciation, as seen just to the north of the location of point G in Figs. 2a, 2b, and 2d. The increase in BTD appears simultaneously with the appearance of glaciation, before there was time available for the cloud to lose condensates as precipitation. Therefore, it is suggested that the BTD signature, which usually indicates decreasing optical depth of the clouds, occurs because of the disappear-

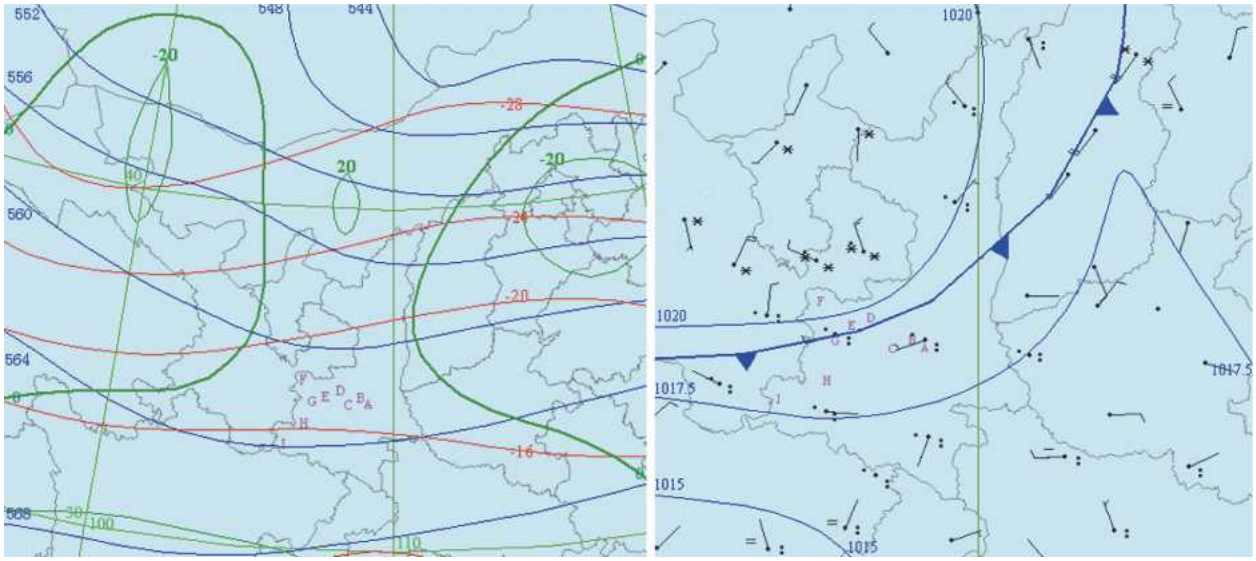

FIG. 5. Synoptic maps at 1200 UTC 14 Mar 2000 of (left) 500 hPa with isotherms (°C, red), geopotential height lines (10 gpm, blue), and vorticity lines (10^{-5} s^{-1}, green). (right) Surface map shows the cold front and weather conditions using the standard synoptic symbols. The turning points of the seeding track are denoted by the characters A–I.

ance of the large number of supercooled cloud droplets on the much smaller number of relatively large ice crystals. This process of coagulation is known to be associated with a decrease in the optical depth for a given water path. It is worth noting that, despite the increased BTD, the visible (0.6 μm) reflectance in the seeded tracks did not decrease at all, and even somewhat increased. This indicates that the clouds were still quite thick and contained much water in various forms. This combination of moderate BTD values with high visible reflectance is typical of mature glaciated precipitating clouds.

The glaciation advances and releases latent heat that causes the air to rise in the middle of the seeded track and form a cloud line of small supercooled droplets just in the middle of the channel that is caused by the sinking of the glaciated cloud tops. This starts shortly after point F, and is seen vividly in Fig. 2a. The age of the seeding track at this point is about 37 min after seeding. The growth of small water clouds inside the seeded track keeps occurring intermittently until point C, which is 62 min after seeding. The disappearance of these midtrack water clouds later suggests that the seeded track has matured and no additional latent heat of freezing is being released. In contrast to the midtrack ridge clouds that appear to form because of the latent heat of freezing at the time of prime development of the seeding track, the maturation of the seeding track is associated with its narrowing and eventual dissipation due to expansion of the tops of the ambient clouds from the sides inward.

The ice particles that compose the top of the glaciated seeded track descend gravitationally, while the warmed air rises and form these new clouds at the middle of the seeding track. The shadow structure indicated that the glaciated cloud top descend about 1500 m within a little more than an hour. This translates to a terminal fall velocity of ~40 cm s^{-1} for the ice particles that compose the cloud top, if the air was vertically still. This terminal fall velocity is typical for plane dendrites, which is the likely crystal habit in these conditions. Langmuir (1961b) also used the shadows for estimating a sinking rate of 30–35 cm s^{-1} for the cloud tops in his dry-ice-seeded tracks that occurred at relatively low heights (~2200 m), and with modest supercooling of about −5°C. The greater fall velocity that is reported here is consistent with the larger ice crystals at the lower temperatures and the lower air density in this study. The forming of the new small water clouds within the seeded track indicates that there is some rising motion of the air, making this velocity the lower bound. Aggregation can take place lower in the seeding track, and the aggregates can fall much faster as snowflakes. Thin clouds start to close again from above on the seeded track with its maturation, as can be seen in segment AB of the track in Fig. 2a. However, deeper in the cloud the glaciation continues to expand, as is evident by the BTD signature (Fig. 2e).

The aircraft operators reported initiation of seeding at point A, but the seeding signature continues back to point O, where the aircraft was circling upward before it had started seeding. Despite that, there is a large apparent seeding signature. Is this due to aircraft-

produced ice particles (Rangno and Hobbs 1983; Woodley et al. 2003), or was the AgI generator actually ignited before reaching point A? In any case, how did the seeding plume expand to the cloud top at 5.3 km from the seeding level of 4 km at point A, or even lower at point O? (see Table 1). The Xian radiosonde of 1200 UTC (located near point O) ascended in the adiabatically moist lapse rate cloudy layer between 3.7 and 5.3 km (from −6° to −17°C), topped by a temperature inversion. In such conditions the latent heat release due to the seeding-induced glaciation probably caused rising motions that could propagate the seeding effect in the moist-adiabatic cloudy layer all the way to the cloud top. We suggest that latent heat was actually released and caused rising motion in the seeded track based on the subsequent formation of the midtrack ridge of clouds. In contrast to these clouds that formed at the time of prime development of the seeding track, the maturation of the seeding track is associated with its narrowing and eventual dissipation because of expansion of the tops of the ambient clouds from the sides inward.

5. Conclusions

Glaciogenic cloud seeding in thick supercooled layer clouds modified them to the extent that can be clearly detected by the operational orbital weather satellites. The retrieved properties of the seeded track suggest that seeding glaciated the cloud through a deep layer and initiated the precipitation processes, as intended. The satellite view allows for observation of the scale of the seeding effects in time and space (the respective scales are hours and hundreds of kilometers). It opens new possibilities of using satellite for directing and monitoring weather modification experiments and operations.

The observed profound impact of the artificially added ice nuclei on the clouds suggests that similar effects can be expected by naturally occurring ice nuclei, such as desert dust particle that can nucleate ice starting at −7° to −11°C. Therefore, it is reasonable to predict that desert dust would glaciate supercooled layer clouds and induce their dissipation by a process of "snow out." This might be applicable also to convective clouds, but this is still an open question. These demonstrated impacts of ice nuclei on clouds have important ramifications on the sensitivity of the hydrological and radiative climate processes to naturally occurring ice nuclei, such as in desert dust, as well as to the scarcely documented anthropogenic ice nuclei.

It is hoped that this demonstration of the use of satellite capabilities to detect glaciogenic seeding effects on supercooled clouds will bring advancement in the field along the same lines as that of the satellite-observed ship tracks, which inspired the development of the field of cloud–aerosol interactions on the properties of marine stratocumulus and their climatic implications.

Acknowledgments. The authors thank Dr. W. L. Woodley for valuable discussions and reviewing the manuscript. The authors are grateful to Mr. Max Zingerman of the Hebrew University, who produced the geographical rectification and 3D rendering of the satellite images, and Mr. Omer Burstein, who processed the satellite data.

REFERENCES

Albrecht, B. A., 1989: Aerosols, cloud microphysics and fractional cloudiness. *Science,* **245,** 1227–1230.

Inoue, T., 1989: Features of clouds over the tropical Pacific during Northern Hemispheric winter derived from split window measurements. *J. Meteor. Soc. Japan,* **67,** 621–637.

Langmuir, I., 1961a: *Atmospheric Phenomena.* Vol. 10, *Collected Works of Langmuir,* Pergamon Press, 477 pp.

——, 1961b: *Cloud Nucleation.* Vol. 11, *Collected Works of Langmuir,* Pergamon Press, 619 pp.

Mason, B. J., 1962: *Clouds, Rain and Rainmaking*. Cambridge University Press, 189 pp.

Rangno, A. L., and P. V. Hobbs, 1983: Production of ice particles in clouds due to aircraft penetrations. *J. Climate Appl. Meteor.,* **22,** 214–232.

Rosenfeld, D., 1999: TRMM observed first direct evidence of smoke from forest fires inhibiting rainfall. *Geophys. Res. Lett.,* **26**, 3105–3108.

——, 2000: Suppression of rain and snow by urban and industrial air pollution. *Science,* **287,** 1793–1796.

——, and I. M. Lensky, 1998: Spaceborne sensed insights into precipitation formation processes in continental and maritime clouds. *Bull. Amer. Meteor. Soc.,* **79,** 2457–2476.

——, and W. L. Woodley, 2003: Closing the 50-year circle: From cloud seeding to space and back to climate change through precipitation physics. *Cloud Systems, Hurricanes, and the Tropical Rainfall Measuring Mission (TRMM), Meteor. Monogr.,* No. 51*,* Amer. Meteor. Soc., 59–80.

——, R. Lahav, A. P. Khain, and M. Pinsky, 2002: The role of sea-spray in cleansing air pollution over ocean via cloud processes. *Science,* **297,** 1667–1670.

Rudich, Y., D. Rosenfeld, and O. Khersonsky, 2002: Treating clouds with a grain of salt. *Geophys. Res. Lett.,* **29,** 2060, doi:10.1029/2002GL016055.

Schaefer, V. J., 1946: The production of ice crystals in a cloud of supercooled water droplets. *Science,* **104,** 457–459.

Silverman, B. A., 2001: A critical assessment of glaciogenic seeding of convective clouds for rainfall enhancement. *Bull. Amer. Meteor. Soc.,* **82,** 903–924.

Woodley, W. L., D. Rosenfeld, and A. Strautins, 2000: Identification of a seeding signature in Texas using multi-spectral satellite imagery. *J. Wea. Mod.,* **32,** 37–52.

——, G. Gordon, T. J. Henderson, B. Vonnegut, D. Rosenfeld, and A. Detwiler, 2003: Aircraft-produced ice particles (APIPS): Additional results and further insights. *J. Appl. Meteor.,* **42,** 640–651.

Yu, X., J. Dai, D. Rosenfeld, H. Lei, X. Xu, P. Fan, and Z. Chen, 2005: Comparison of model-predicted transport and diffusion of seeding material with NOAA satellite-observed seeding track in supercooled layer clouds. *J. Appl. Meteor.,* **44,** 749–759.